THE ROLE OF RIP3 IN NEUROINFLAMMATION IN THE POSTNATAL MOUSE BRAIN

A Thesis

by

DAVID C. GILLIS

Submitted to the Office of Graduate and Professional Studies of
Texas A&M University
in partial fulfillment of the requirements for the degree of

MASTER OF SCIENCE

Chair of Committee,	Jianrong Li
Committee Members,	Louise C. Abbott
	Rajesh C. Miranda
Head of Department,	Evelyn Tiffany-Castiglioni

August 2015

Major Subject: Biomedical Sciences

ABSTRACT

Inflammation in the developing central nervous system (CNS) can contribute to numerous issues in the fully developed adult. Uncovering pathways responsible for the inflammation is valuable for future intervention strategies aimed at preventing or reducing inflammation. Receptor interacting protein kinase 3 (RIP3) has recently been identified as a critical signaling molecule in initiating programmed necrosis (also termed necroptosis), which may contribute to cell damage and subsequent inflammation under pathophysiological conditions such as stroke and traumatic injury. The goal of this study was to use genetic approaches to determine the role of RIP3 in brain immune responses after systemic inflammatory challenge and the contribution of RIP3 to inflammation-induced potentiation of hippocampal injury in an ex vivo model of hypoxia/ischemia. Stimulation with lipopolysaccharide (LPS) elicited robust proinflammatory responses of organotypic hippocampal slices and significantly exacerbated CA1 neuronal excitotoxicity after subsequent oxygen glucose deprivation (OGD). Genetic ablation of RIP3 resulted in decreased levels of interleukin-1β (IL-1β) after LPS stimulation and suppressed excitotoxicity after subsequent OGD challenge. These results suggest that activation of RIP3 increases proinflammatory responses in cultured hippocampal slices. To determine if RIP3 regulates inflammation in vivo, we examined cytokine and chemokine levels of the brain after subcutaneous LPS administration followed by hypoxia in early postnatal pups. Mice lacking RIP3

produced significantly lower levels of proinflammatory cytokine IL-1β 6-24 hours after LPS administration when compared to wildtype *RIP3*$^{+/+}$ littermates. In contrast, 4 and 21 days after LPS administration followed by hypoxia, IL-1β and other proinflammatory cytokine transcript levels in the brain were drastically diminished and were comparable between *RIP3*$^{+/+}$ and *RIP3*$^{-/-}$ mice. Our preliminary data suggest that these *RIP3*$^{-/-}$ mice show lower expression of genes responsible for myelination. In summary, our results demonstrate, for the first time, that RIP3 mediates proinflammatory responses in the CNS by enhancing IL-1β production and imply that RIP3 is a potential target for neuroinflammatory disorders.

DEDICATION

This work is dedicated to my family. To my parents who frequently told me that I must work hard to obtain this degree. To my grandmother who repeatedly told me that there are two things in life that I must choose, my job and my wife. To my sister who always gave me good reasons to go after what made me happy, and for always putting up a good fight against her big bully brother. Finally, to the research team that worked daily to help me along the way to learning all of the skills and knowledge necessary to successfully complete a Master of Science degree.

ACKNOWLEDGEMENTS

My sincere gratitude goes to my committee members: Dr. Jianrong Li, Dr. Louise Abbott, and Dr. Rajesh Miranda for their guidance, support, encouragement, and motivation. I especially thank Dr. Li for providing me with a great opportunity to complete a Master's degree under her guidance. I am forever grateful for her excitement and passion for neuroscience research. In addition, I appreciate all of the mentoring and guidance provided from all of my lab members: Sunja Kim, Andrew Steelman, Yu Kong, and Felix Lu, all contributors to my education as a graduate student. Finally, I acknowledge research collaborators: Dr. Xiaodong Wang at the National Institute of Biological Sciences in Beijing for the wonderful gift of the RIP3 knockout mouse line and also Dr. Q. Richard Lu at UT Southwestern for transgenic mice used in cell imaging studies. Thank you to the Texas A&M College of Veterinary Medicine and the Office of Research and Graduate studies for providing funding for my research and funding to travel to high impact conferences in my field of study.

NOMENCLATURE

ANOVA	analysis of variance
Ara-C	cytosine b-D-arabinofuranoside
CA1	region 1 of hippocampus proper
CC1	APC immunogen clone CC1
CCL2	chemokine ligand 2
CCL3	chemokine ligand 3
CCL5	chemokine ligand 5
cDNA	complementary deoxyribonucleic acid
CNP	2',3'-Cyclic-nucleotide 3'-phosphodiesterase
CNS	central nervous system
CV	cresyl violet
DMEM	dulbecco's modified eagle medium
DMFI	change in mean fluorescent intensity
DNA	deoxyribonucleic acid
EBSS	earl's balanced salt solution
EDTA	ethylenediaminetetraacetic acid
FBS	fetal bovine serum
GFAP	glial fibrillary acidic protein
H + E	haematoxylin and eosin

IACUC	institutional animal care and use committee
IHC	immunohistochemistry
IL-18	interleukin 18
IL-1b	interleukin 1 beta
IL-6	interleukin 6
LDL	low density lipoprotein
LME	L-leucine methyl ester
LPS	lipopolysaccharide
MAG	myelin associated glycoprotein
MAP2	microtubule-associated protein 2
MBP	myelin basic protein
MEM	minimal essential medium
mRNA	messenger ribonucleic acid
NB	neurobasal
Nec-1	necrostatin 1
NLRP	NACHT, LRR, and PYD domains-containing protein
NMDA	N-methyl-D-aspartic acid
ns	not significant
OGD	oxygen glucose deprivation
P/S	penicillin/streptomycin
PBS	phosphate buffered saline
PCR	polymerase chain reaction

PDL	poly-D-lysine
PFA	paraformaldehyde
PI	propidium iodide
PLP	proteolipid protein
qPCR	quantitative polymerase chain reaction
RHIM	receptor interacting homotypic interacting motif
RIP1	receptor interacting protein 1
RIP3	receptor interacting protein 3
ROS	reactive oxygen species
RT-qPCR	reverse transcription-quantitative polymerase chain reaction
SDM	slice dissection medium
SEM	standard error of the mean
SFM	serum free medium
TAMU	Texas A&M University
TLR	toll-like receptor
TNF-a	tumor necrosis factor alpha

TABLE OF CONTENTS

LIST OF FIGURES

LIST OF TABLES

CHAPTER I

INTRODUCTION

The CNS is solely dependent upon oxygen consumption, and consumption occurs at a very high rate. In this oxygenated environment, increased reactive oxygen species (ROS) production is counter balanced with various defense mechanisms that remove ROS and related metabolites. Overproduction of ROS results in oxidative stress, which has been linked to many diseases (Finkel and Holbrook, 2000) and can cause programmed cell death (Vandenabeele et al., 2010a). In addition, prior work reveals an importance of inflammation along with oxidative stresses, which lead to injury (Sheldon et al., 2004, Barks et al., 2008). Our overall hypothesis is that reduced oxygen combined with inflammation carries heavy consequences to the development of the brain.

Hypoxia and systemic inflammation in the developing brain

During one of many scenarios, inflammation can occur when cells undergo death by means of necrosis because they spew their contents into the extracellular environment. This can be reduced by antioxidants such as vitamin E and other members of this family (Ahn et al., 2007). Clinical and experimental studies have shown that hypoxia/ischemia and maternal/fetal infection are risk factors for the developing brain (Rousset et al., 2006, Rousset et al., 2013). In neonates, a hypoxic and ischemic environment causes pathology that is visible starting 3 hours up to 100 days after insult with massive tissue injury and atrophy including activated glial cells. This could lead to

cerebral palsy and cognitive impairments that can also alter social skills, attention span, and overall behavioral alterations (Shrivastava et al., 2012). Systemic inflammation triggered by *E. coli* exacerbates hypoxic/ischemic brain injury and leads to myelination deficits (Loron et al., 2011) and damage to healthy cells in the developing brain, which is most likely due to aberrant innate immune responses in the brain. There exist many possible avenues for activating the innate immune system, and in all of these possibilities, the developing brain becomes increasingly susceptible to brain injury. For example, the developing brain becomes more susceptible to cerebral palsy, along with various abnormalities occurring in the white matter (Mallard and Wang, 2012). Others use LPS, a cell wall component of gram-negative bacteria to show that systemic inflammation can lead to long term neurological consequences such as motor dysfunction (Rousset et al., 2013), and white matter damage (Favrais et al., 2011). Activation of N-methyl-D-aspartate (NMDA) receptors on microglia are activated (by LPS for example), which results in release of proinflammatory cytokines and factors that cause neuronal cell death (Kaindl et al., 2012).

Role for RIP3 in regulated necrosis and inflammation

RIP3 is the third member of a family of receptor interacting proteins and is found on chromosome 14 (Kasof et al., 2000). This protein was named as a part of this family when initial experiments using a yeast two hybrid screen found it to bind to receptor interacting protein 1 (RIP1) (Yu et al., 1999). RIP3 was also found to be involved in activation of proinflammatory signaling pathways (Pazdernik et al., 1999, Sun et al., 1999). RIP3, through its receptor interacting homotypic interacting motif (RHIM),

interacts with RIP1 (Sun et al., 2002) (Figure 1) and the formation of RIP1/RIP3 complex and RIP1 kinase activity have been shown to be critical in initiating programmed necrosis (Figure 2), which challenged the central dogma that apoptosis was the only means of programmed cell death and ignited prolific research interest in the field (Vandenabeele et al., 2010b, Ofengeim and Yuan, 2013).

The small molecule named necrostatin-1 (Nec-1) that targets the kinase activity of RIP1 (Degterev et al., 2005, Degterev et al., 2008) has been shown to significantly decrease injury and infarct size in ischemic kidney (Linkermann et al., 2012), heart (Oerlemans et al., 2012), and brain (Northington et al., 2011). Administration of nec-1 also significantly reduced cell death when given promptly after hypoxia/ischemia (Chavez-Valdez et al., 2012, Linkermann et al., 2012). These studies suggest that programmed necrosis may contribute to ischemic brain tissue damage.

Later subsequent studies from three independent groups simultaneously identified RIP3 in acting as a "master switch" of tumor necrosis factor alpha (TNF-α)-induced cell death from apoptosis to necrosis (Cho et al., 2009, He et al., 2009, Zhang et al., 2009). Given that Nec-1 is protective against ischemic brain damage and that RIP3 interacts with RIP1 and is critical in triggering necroptosis, a genetic approach with *RIP3*$^{-/-}$ mice would bypass potential off-target effects of nec-1 in vivo (Vandenabeele et al., 2013) and provide valuable insights into the potential function of RIP3 during ischemia and inflammation in the CNS.

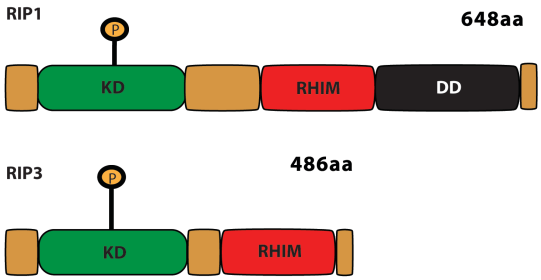

Figure 1 *The similarities and differences between receptor interacting proteins*. Both proteins have a kinase domain (KD), and RIP homotypic interacting motif (RHIM) while RIP3 lacks a death domain (DD).

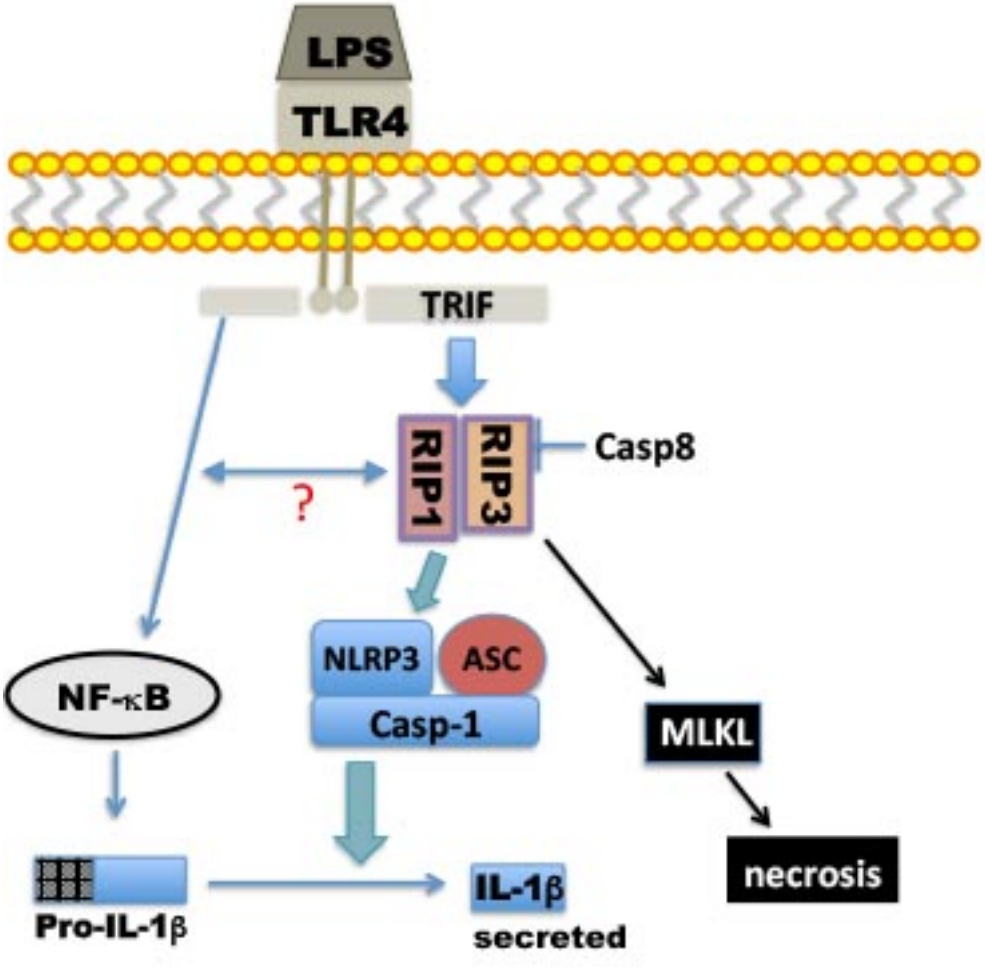

Figure 2 *Signaling pathways involving RIP3.* The following cartoon depicts the simplified involvement of RIP3 in pathways leading to inflammation.

Experimental model systems used in our studies

Maternal exposure to LPS during gestation causes hypomyelination, programmed cell death of all cells in specific areas of the fetus (Rousset et al., 2006), and activation of NMDA receptors on microglia (Kaindl et al., 2012). Since maternal exposure to LPS produces injury during postnatal development, we used a mouse line where RIP3 gene is ablated (He et al., 2009) to determine if RIP3 regulates brain immune responses followed by the outcome of systemic LPS exposure to newborn mouse pups. A well-established experimental model (Nobuta et al., 2012) was adapted for this current study. Briefly, a certain regime of LPS administration at particular times induces white matter damage. In addition, we employed organotypic slice cultures, which maintain synaptic connections and preserve the relevant stoichiometry of the glia and neurons (Sundstrom et al., 2005), to establish an in vitro inflammation and oxygen glucose deprivation (OGD) model to partially mimic the in vivo systemic LPS injections in RIP3 null postnatal mice. The overall goal of this study is to investigate how the CNS immune response is regulated during early postnatal brain development and, to our knowledge, is the first to use a genetic RIP3 mutant mouse line to examine the immune responses in the developing CNS after systemic inflammation.

CHAPTER II

MATERIALS AND METHODS

Materials

Earl's balanced salt solution (EBSS), hank's balanced salt solution (HBSS), dulbecco's modified eagle medium (DMEM) with high glucose, and fetal bovine serum (FBS) were purchased from Hyclone (Logan, UT). Neurobasal Medium (NB) and B27 supplement were purchased from Gibco/Life Technologies (Carlsbad, CA). Antibodies against RIP1 and RIP3 were purchased from R&D Systems (Minneapolis, MN) and Imgenex (San Diego, CA) respectively. Hoechst 33342 for nuclei staining and Alexa 488 and 594 was from Invitrogen (Carlsbad, CA). Rabbit monoclonal anti-microtubule-associated protein 2 (MAP2) antibody was purchased from Cell Signaling Technology (Danvers, MA). Glial fibrillary acidic protein (GFAP) and APC immunogen clone CC1 (CC1) were purchased from Calbiochem (Billerica, MA). Rat monoclonal anti-CD68 antibody was purchased from AbD Serotec (Raliegh, NC). Rabbit polyclonal anti-Iba-1 antibody was purchased from Wako Chemicals (Richmond, VA). Antibodies to nestin, TBR2, and Olig2 were purchased from Millipore (Billerica, MA). All other reagents used were purchased from Sigma-Aldrich (St. Louis, MO).

Genotyping

Mice used were generated as described by (He et al., 2009). Tissue for genotyping was obtained from the last centimeter of the animal's tail. Tail clips were

then digested in tissue digestion buffer (50 mM Tris 20 mM NaCl 1 mM EDTA 1% SDS 0.5 mg/ml Proteinase K) for 20 minutes at 55^0 C. Then 200 µL of water was added to each sample and boiled for 5 minutes. After 10 minutes at 14,000 rpm, the supernatant DNA was quantified using a Nanodrop 1000 photospectrometer, and 50 ng of DNA per reaction was used for PCR. PCR with RIP3 gene specific primers (Table 1) was carried out as follows: an initial denaturing step for 2 minutes at 94^0 C, followed by 35 cycles of three steps (94^0 C for 30 seconds, 60^0 C for 30 seconds, 72^0 C for 60 seconds) and a final elongation step at 72^0 C for 10 minutes. Samples were then run in a 1% agarose gel for 30 minutes at 130 volts (constant) and then imaged using Chemidox XRS gel documentation system (Bio-rad Hercules, CA). One of three different outcomes for genotype was possible based on PCR product size as shown below (Figure 2).

Table 1 *Genotyping primer sequences*. Targeted for mouse (Newton et al., 2004).

Primer Name	Sequence (5' to 3')
RIP3 Fwd	ACATGCATGGTCATGCACACACAT
RIP3 Rev WT	TTGAGACAGGGTCTCTTTTTGGAG
RIP3 Rev KO	GTCGAGGGACCTAATAACTTCGTA

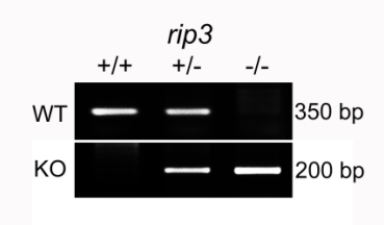

Figure 3 *PCR product size and distribution based on genotype*. Agarose gel visual of PCR product size obtained based on animal genotype.

Primary astrocytes

Astrocytes were prepared using previously described methods (Li 2008). Once meninges were removed under a stereo dissection microscope, the brain tissue was digested using HBSS with 0.01% Trypsin and 10μg/ml DNAse for 15 minutes at 37^0 C. Tissue was then re-suspended and washed twice with DMEM plus 10% FBS and 1% penicillin/streptomycin (P/S). Following the second wash, cells in suspension were passed through a 70 micron nylon cell strainer onto poly-D-lysine (PDL) coated 75 cm^2 flasks. Media [DMEM, 10% FBS, and 1% P/S] was changed every other day for a week. On the seventh day, microglia and pre-oligodendrocytes (pre-OLs) were removed from the culture by shaking at 200 rpm for 13-15 hours in a 37^0 C incubator. The same procedure was repeated a week later. To purify the astrocytes from any remaining microglia, a specific toxin to microglia called L-leucine methyl ester (LME) (1mM) was incubated with the monolayer for 1h at 37^0 C. Astrocytes were then split, re-plated to a lower density in DMEM 10% FBS 1% P/S, and allowed to proliferate for three days. After proliferation, the astrocytes were treated with LME again for one hour at 37^0 C, washed twice with PBS, centrifuged at 0.1 relative centrifugal force (rcf), re-suspended

in D10S, and plated onto 96 well, 8 well chamber slides, or 24 well plates at 5.0 X 10^4 cells /mL.

Primary neurons

Adult Sprague-Dawley rats or C57/B6 mice at E16 stage of pregnancy were euthanized according to a procedure approved by Texas A&M University institutional animal care and use committee (TAMU IACUC). Following euthanasia, an incision was made in the abdominal region to remove the embryo sacs. Once obtained, microdissection scissors were used to remove each embryo from the sac followed by removing the brain from the embryo. Brains were then placed into cold HBSS inside a 10 cm petri dish on top of an ice pack. The meninges were removed with fine forceps under a stereo dissection microscope inside of a laminar flow hood. The brain was then separated into regions and only the cortical and hippocampal regions were used while the midbrain and hindbrain was discarded. These brain tissues were then digested for 5 minutes inside a 37^0 C water bath using 5 mg of freshly prepared papain in HBSS. To stop the activity of papain, tissues were incubated with 10mg/ml trypsin inhibitor 3 times total, each with 3 minute incubation in the 37^0 C water bath. DMEM containing glutamine and 10% FBS was then used to titrate out the suspension until it was homogenous with no clumps. This suspension was then passed through a 70 micron cell strainer into a 50 mL falcon tube. Cells were diluted to a final density of 2.5 X10^5 cells/cm^2 and plated into 96 well plates for experiments. The next day, the media was carefully removed, rinsed out with phosphate buffered saline (PBS), and replaced with NB medium plus B27 supplement containing 3mM Cytosine b-D-arabinofuranoside

(Ara-C). Treatment with Ara-C for 72 hours gave highly purified neuronal cultures and at day 3 in vitro (DIV3), the medium containing Ara-C was replaced with NB Medium plus B27 supplement. Every other day thereafter, half changes of the media were performed until the cells were ready for experiments. Immature neuronal cultures between DIV4 to DIV6 were used for all experiments.

Immunocytochemistry and immunohistochemistry with fluorescence microscopy

Before obtaining brain tissue, each mouse was transcardially perfused using PBS. However, if the mouse was aged less than postnatal day 7, no perfusion was carried out. Obtained brain tissues were then fixed in 4% paraformaldehyde (PFA) for 12-24 hours at 4^0 C, cryoprotected with 30% sucrose in PBS, and cut into 10 micron sections and placed onto plus coated glass slides. Using PBS, tissue sections were rinsed 3 times total, allowing 5 minutes of incubation for each rinse. Next, cells were blocked and permeabilized using 5% goat serum and 0.3% Triton X in PBS for 1 hour at room temperature. Once blocking was complete, the slide was rinsed once with PBS. Next, the primary antibody was diluted to desired concentration in PBS with 0.1% Triton X. The following antibodies were used: GFAP at 1:300, Iba-1 at 1:300, CC1 at 1:200, Nestin at 1:100, TBR2 at 1:100, Olig 2 at 1:1000, and CD68 at 1:100. This was then added to the slide, and allowed to incubate overnight at 4^0 C. The next day, the slide was rinsed 3 times for 5 minutes each using PBS. Then the respective secondary antibody conjugated to either Alexa 488 or 594 was used at a1:1000 dilution. This mixture was added to the slide and incubated for 1 hour at room temperature. Following secondary antibody incubation, the slide was washed 3 times for 5 minutes each using PBS. The final wash

used Hoechst 33342 added at a 1:10,000 dilution in order to label the nuclei. After 5 minutes, this mixture was rinsed out and then PBS was added to the slide. Next, the cultures were imaged for analysis and nuclei cell counting.

Organotypic hippocampal slice cultures

5 to 6 day old mice were anesthetized and decapitated followed by removal of the whole brain. The first 1-3 mm of each hemisphere was removed from the anterior portion and the entire cerebellum and brainstem from the posterior portion. Using a sterile razor blade, the brain was divided into the left and right hemisphere. The whole brain was super glued anterior side down onto the stage of the vibratome (Leica model VT1200) and immersed into ice-cold slice dissection medium (SDM) [EBSS with 25 mM HEPES, 1.8 mM CaCl2, 0.813 mM MgSO4]. Starting from the posterior end, 400 micron slices were cut with the vibratome set to 1.80 mm amplitude and 0.05 mm/sec. Slices were transferred to a 100 cm petri dish containing SDM, which was chilled using an ice pack placed on a stereo dissection microscope. Under the stereo dissection microscope, using a set of bent and dulled half inch 27 gauge needles attached to 1 mL syringes, the cortical region was detached from the hippocampus. All other structures besides the hippocampus were trimmed away so that only the hippocampus remained. Using a plastic transfer pipet, the hippocampi were transferred to 50 mL conical tubes containing SDM and placed on ice for 15-30 minutes. Next, slices were transferred onto Millicell membrane inserts in a 6 well plate placed in 1 mL of slice feeding medium (SFM) [50% minimum essential medium (MEM), 25% EBSS, 25% heat-inactivated horse serum, 2 mM GlutaMAX-I, 5 mg/ml D-Glucose, 100 U/ml P/S, and 1 μg/mL

Fungizone at pH 7.2]. These slices were grown for 9 days before experimental use. Every other day, half the media was removed and replaced with fresh media.

Oxygen glucose deprivation (OGD)

After 8 days in culture, slices were pre-treated with 1 μg/ml LPS and 1 μg/ml propidium iodide (PI). PI was incorporated into all the media for the entire experiment and is used to trace dying cells. 24 hours later, after three washes with PBS, hippocampal slices were subjected to OGD in glucose-free SFM where glucose was replaced with an equal concentration of sucrose. This media lacking glucose was bubbled with 95% N_2 and 5% CO_2 gas for 30 minutes to remove the oxygen. The slices were washed three times with this media for 10 minutes each. The slices were then placed into a hypoxia chamber, which was sealed to be air tight and flushed with N_2 gas to remove all oxygen. After ten minutes of N_2/CO_2 flushing (twenty 30 second cycles), the chamber was sealed and placed into the 37^0 C incubator for 45 minutes. Normoxia control slices were given the same media formulation with the addition of 25 mM glucose and normal oxygen environment. Following this incubation, the slices were given glucose containing SFM (without serum) and allowed to recover for 24 hours. Slices were then imaged for PI fluorescence under the microscope.

Subcutaneous lipopolysaccharide (LPS) administration and hypoxia

LPS was purchased from Sigma (E. coli strain 011:B4) and determined that 1 mg/kg body weight was sufficient to consistently cause inflammation after 2 subcutaneous injections between each shoulder. LPS was diluted in sterile PBS and administered subcutaneously in a volume of 20 μL. Pups at postnatal day 2 and weighing

between 1.5 to 1.8 grams were used for these administrations (Nobuta et al., 2012). If the animals fell below this weight limit, there was a 12-15 hour waiting period before the first administration was given. Between 15-17 hours after the first injection, the second injection was given on the opposite shoulder. There were two experimental groups: One group of animals was sacrificed 24 hours after the first injection. The second group examined the effects of 1 hour with hypoxia (92% N_2 and 8% O_2). The animals in the second group were subjected to hypoxia (8% O_2, 1 hour) 8 hours after the second injection, and were then returned to the dam for an additional 48 hours, 10 days, or 21 days. At the respective time points, the animals were sacrificed and their brain was used for further analysis. The brain was split into two hemispheres. One hemisphere was flash frozen in liquid nitrogen to be used for mRNA analysis while the other hemisphere was fixed in 4% PFA, cryoprotected in 30% sucrose, and sectioned for immunohistochemical analysis.

RNA isolation and RT-qPCR

RNA was extracted from brain hemisphere tissue using TRI Reagent® (Sigma, St. Louis, MO) according to manufacturer's instructions. Quantified nucleic acids obtained from this procedure were then converted to cDNA as follows. The contaminating DNA was digested and removed using DNase I kit (Life Technologies Carlsbad, CA) followed by reverse transcription using AMV kit (Promega Madison, WI). To check for successful reverse transcription, PCR using 100 ng cDNA was performed to verify amplification. For qPCR, 10 ng of cDNA was used to amplify the following genes (Table 2). The SYBR dye was used according to manufacturer's

instructions (Life Technologies, Grand Island, NY). All samples were run using a CFX384 Touch™ Real-Time PCR Detection System (Bio-Rad, Hercules, CA) in duplicate. Gene expression was normalized to β-actin expression. Fold expression was calculated using the formula $2^{-\Delta\Delta Ct}$ (Livak and Schmittgen, 2001).

Table 2 *qPCR primers.* Primers made using mouse genes.

Gene	Forward (5' to 3')	Reverse (5' to 3')
CNP	AGGAGAAGCTTGAGCTGGTC	CGATCTCTTCACCACCTCCT
MAG	GATGATATTCCTCGCCACC	ACTGACCTCCACTTCCGTT
MBP	CACACACGAGAACTACCCA	GGTGTTCGAGGTGTCACAA
CCL2	GGCTCAGCCAGATGCAGTTA	GCTGCTGGTGATCCTCTTGT
CCL3	CCGGAAGATTCCACGCCAAT	GTCTCTTTGGAGTCAGCGCA
CCL5	GCCAGCTTGGGGATGCCACTC	CAGAGCCTCGGAGCAGCTGAG
TNFα	TGTCCCTTTCACTCACTGGC	CATCTTTTGGGGGAGTGCCT
IL-1β	CGACAAAATACCTGTGGCCT	TTCTTTGGGTATTGCTTGGG
IL-6	TGGTGACCACGGCCTTCC	AGCCTCCGACTTGTGAAGTGGT
β-actin	ATGTGGATCAGCAAGCAGGA	AAAGGGTGTAAAACGCAGCTC
IL-18	ACGTGTTCCAGGACACAACA	ACAAACCCTCCCCACCTAAC
IL-10	TGAGGATCAGCAGGGGCCAGT	CTGGCTGAAGGCAGTCCGCA
RIP3	GCCTTCCTCTCAGTCCACAC	CTTTGCCCACAAACTCCAGC

Image analysis- cell counts and fluorescence intensity analysis

Fluorescent intensity of PI positive cells in the CA1 region of hippocampal slice cultures was used to determine neuronal cell death. In addition, sagittal sections of one hemisphere of the mouse brain were used to count Iba-1 and CC1 positive cells in the hippocampus region. Images were obtained using an Olympus IX71 microscope and Olympus DP70 digital camera at equal exposure. Using ImageJ, background was subtracted, and images were converted to binary followed by measuring the pixel intensity. The intensity value at 24 hours was subtracted from the intensity value at 0 hours to determine the change in mean fluorescent intensity (ΔMFI). To determine Iba-1^+ and $CC1^+$ cell numbers, the images with the respective marker were merged with a Hoechst 33342 image of the same spot. The merged images were used for analysis by first measuring the area of the hippocampus (as mm^2) and counting the nucleated Iba-1^+ and $CC1^+$ cells in each field. The resulting data was expressed as cells/mm^2.

Use of laboratory animals

All protocols for animal use were approved by the TAMU IACUC prior to the start of experiments.

Statistics

All graphs are shown as means $\pm$ standard error (SEM). To determine if differences existed between groups we used one-way analysis of variance (ANOVA) followed by Bonferroni's post-hoc test. All calculations to determine significance were made using GraphPad Prism 4 (GraphPad Software, San Diego, CA). If $p<0.05$, then we considered this a significant difference while $p>0.05$ was considered not significant (ns).

CHAPTER III

RESULTS

RIP3 is predominantly expressed in microglia

We obtained lysates from the purified primary cultures of respective cell type from neonatal rat brain: microglia, oligodendrocytes, neurons, and astrocytes. The lysates obtained from cultures were used for Western blot analysis. We determined that microglia are the cells that produce the highest level of RIP3 protein within the CNS (Figure 4A). The relative amount of RIP3 protein is also highest in microglia. We see that this is the case and in agreement with the visual of the western blot experiment We arrived at this conclusion when we compared RIP3 signal to uniform and unchanged levels of β-actin signal (Figure 4B).

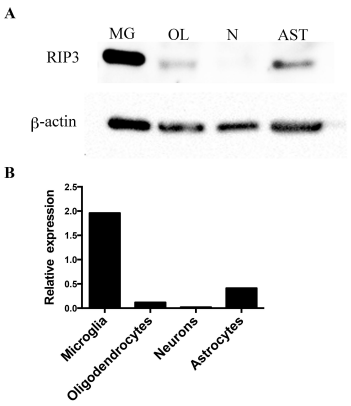

Figure 4 *Microglia predominantly express RIP3*. (A) Western Blot analysis of lysates from primary microglia (MG), oligodendrocytes (OL), mature neurons (N), and astrocytes (AST) using antibodies against RIP3 and b-actin. (B) Relative expression of RIP3 protein compared to loading control β-actin reveals microglia as predominant producer of RIP3.

RIP3 reduces excitotoxicity in a hippocampal slice culture model

We used hippocampal organotypic brain slices from postnatal day 4.5 mice and subjected these tissues to an in vitro experimental OGD paradigm as shown in Figure 5A. The slices were incubated with medium containing 1 μg/ml PI to trace dying cells over the course of experiment. In order to determine that the media formulation was safe for culturing, we used glucose-free OGD media supplemented with 25 mM glucose and found no difference in PI signal after 24 hours. In addition, LPS itself had minimum toxicity on the slice cultures (Figure 5B). This glucose-free OGD media was used during the duration of OGD. At all other times before and after OGD, we used serum free slice feeding glucose-containing media. To examine the effect of inflammation on OGD treatment, we first established a mild OGD toxicity paradigm to produce limited neurotoxicity. To determine a potentiation effect of innate immune responses by microglia, LPS pretreatment was performed. Slices were incubated with 1 μg/ml LPS for 24 hours, washed twice with OGD media, and then subjected to 45 minutes of OGD. The neurotoxicity was significantly higher with LPS pretreatment as seen by significant increase in the number of PI positive cells (Fig. 5C, D), and this neurotoxicity was completely abolished by MK-801, indicating that OGD induces NMDA receptor dependent excitotoxicity (Figure 5C, 5D). The results suggest that neurotoxicity caused by OGD is mediated primarily through NMDA receptors, which cause neuronal cell death. In addition, pretreatment of slices with LPS for 24 hours prior to OGD markedly potentiates the effect of neurotoxicity caused by OGD, and LPS per se does not contribute to the neurotoxicity.

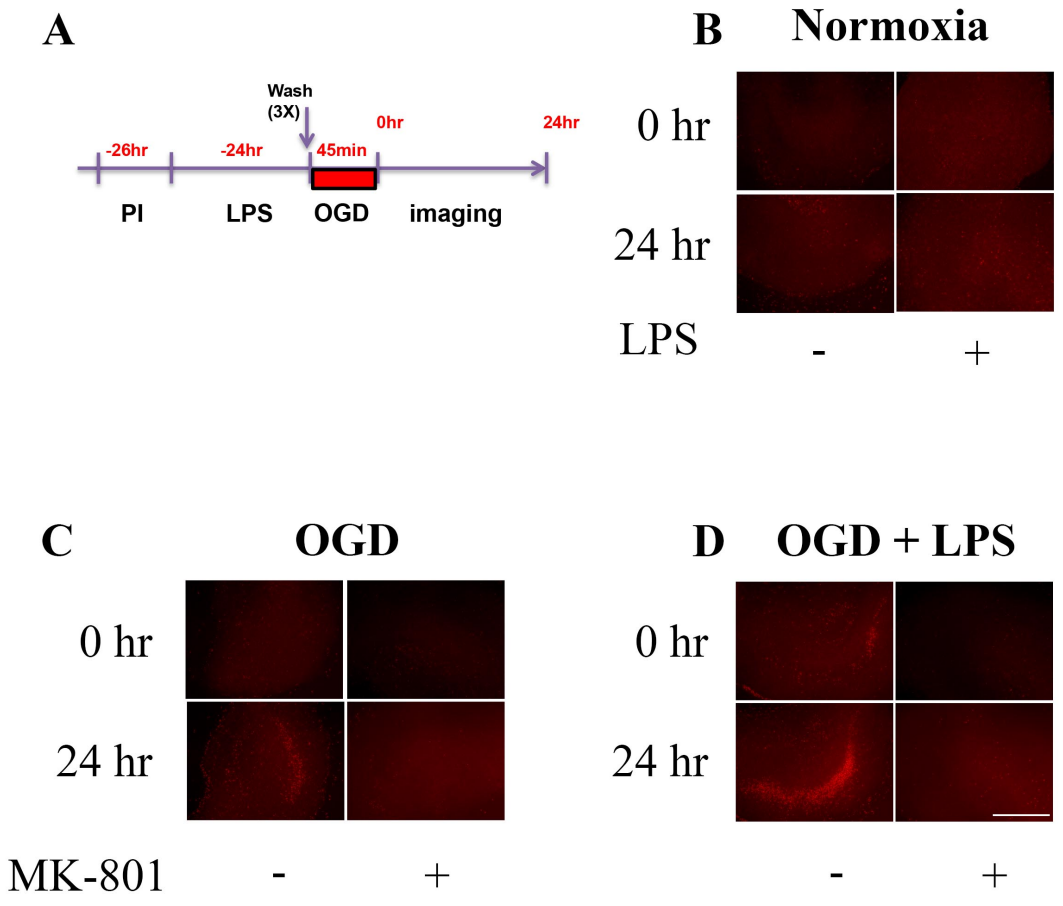

Figure 5 *OGD in slice cultures is potentiated by LPS and blocked by MK-801.* (A) experimental timeline for slice cultures kept nine days in vitro prior to performing OGD. (B) OGD media supplemented with glucose causes no cell death to slice cultures incubated with this media for 45 minutes. (C) Slice cultures exposed to oxygen-limited environment with no glucose in the media undergo excitotoxic cell death in the CA1 region without NMDA receptor antagonist MK-801 and are protected in the presence of MK-801. (D) Slices pretreated with LPS followed by OGD show potentiated cell death in the CA1 region without MK-801 but are protected when MK-801 is present. Images representative from nine animals with three slices per condition from each animal in three independent experiments. Scale bar, 200 microns.

Genetic ablation of RIP3 ameliorates LPS potentiation of OGD induced excitotoxicity

Hippocampal slices cultured for 9 days in vitro (DIV 9) from wildtype, heterozygous, and knockout mice were examined after 24 hours of pretreatment with

LPS and followed by administration of OGD. The slice cultures from wildtype animals, which have both alleles for RIP3 show the most severe injury of the three groups while the heterozygous show moderate injury and the knockout show a significantly lower extent of injury to the CA1 region (Figure 6A). These findings are shown when quantified using ΔMFI, and a significant difference is seen (Figure 6B). In addition, we collected supernatant from slice cultures 24 hours after OGD and saw increased production of the cytokine TNF-α after LPS pretreatment, and showed a lower trend in the knockout cultures (Figure 6C). The results obtained here suggest that in the absence of RIP3, LPS-induced potentiation of OGD neurotoxicity is ameliorated in the CA1 region of the hippocampus.

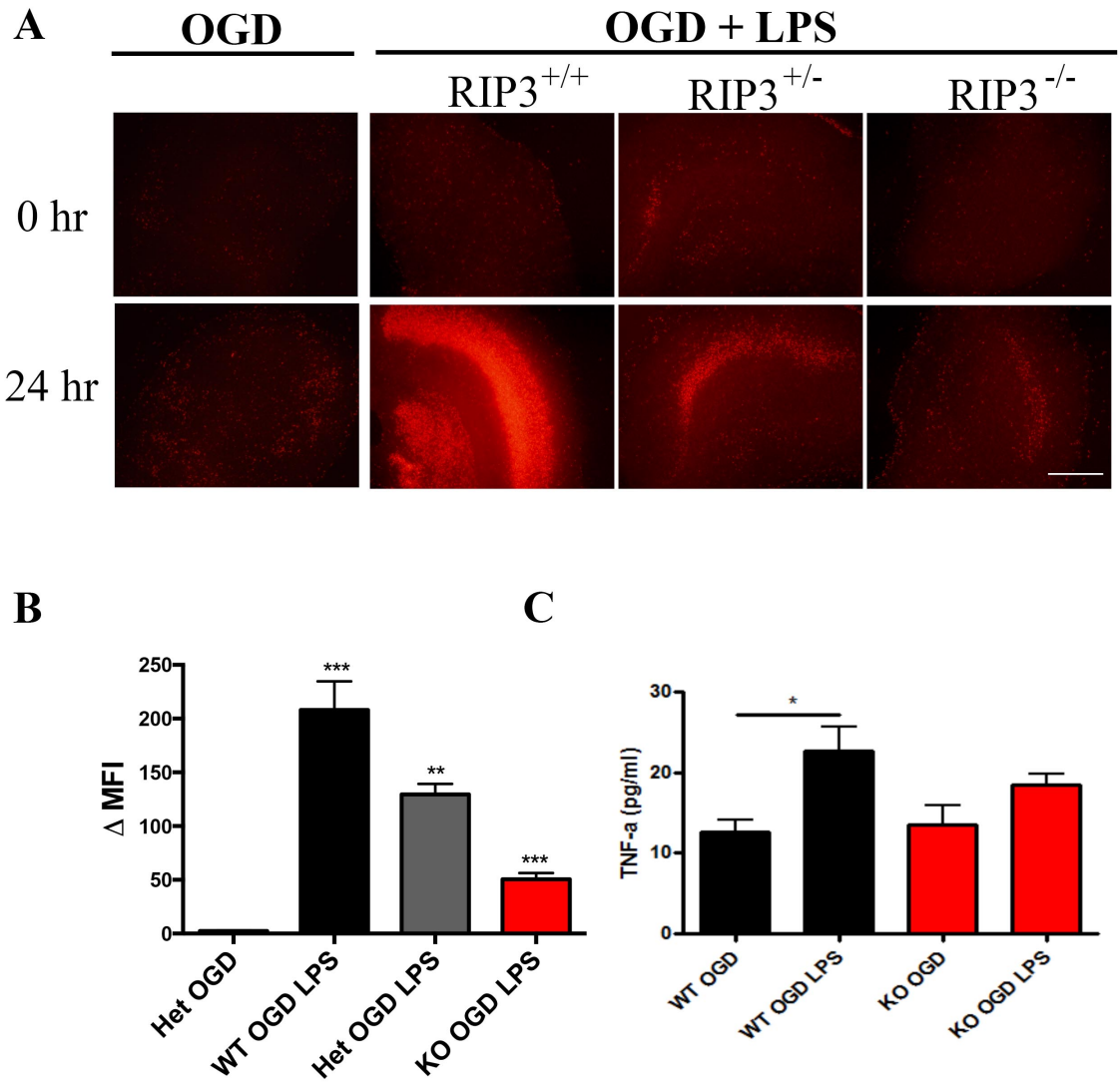

Figure 6 *RIP3 deletion protects hippocampal slice cultures after OGD.* (A) potentiated excitotoxicity with LPS pretreatment in all groups compared to OGD alone and increasingly reduced excitotoxicity in CA1 region when RIP3 is genetically deleted (B) Change in mean fluorescent intensity measurements of the CA1 regions in at least 3 animals per genotype immediately after OGD until 24 hours after OGD (C) Cytokine TNF-α levels of slice cultures 24 hours after OGD show a significant increase in the wildtype with LPS pretreatment as expected while lack of RIP3 shows only a slight increase. Results are combined means ± SE *P<0.05, **P<0.01, ***P<0.001. Each group represents 3 slices from three mice and three independent experiments. Scale bar, 200 microns.

Systemic LPS administration increases CNS cytokine production within 24 hours in part through a RIP3-mediated pathway

RIP3 wildtype and knockout mouse pups at postnatal day 2 were weighed, and pups weighing between 1.4-2.0 grams were given two 20 ml 1 mg/kg subcutaneous LPS injections in the shoulder region. The first injection was given at P2 and 17 hours later, the second injection was given on the opposite side. The total amount of LPS received by each pup was about 3.3 μg. The pups were then returned to the dam for an additional 6 hours. 24 hours after the first injection, the animals were sacrificed and their brain was dissected out for use in frozen sectioning and RNA isolation. The experimental timeline is shown below (Figure 7A).

Each animal was anesthetized then the brain was dissected and one hemisphere was fixed and cryoprotected while the other was flash frozen in liquid nitrogen. RNA extracted from the flash frozen hemisphere was used to determine changes in cytokines and chemokine transcripts using qPCR. Examination of seven proinflammatory cytokines and chemokines revealed changes in expression in the brain after systemic LPS administration. LPS administration causes a significant increase in TNF-α in wildtype but much less degree in knockout and there is an increase in wildtype compared to knockout (Figure 7B). In addition, LPS causes a significant increase in IL-1β in wildtype but not knockout and there is a significant increase in wildtype compared to knockout (Figure 7C). IL-6 is significantly increased in knockout animals administered LPS, but not in wildtype (Figure 7G). Systemic LPS administration causes a significant increase in production of CCL2 for both wildtype and knockout with no

significant change between genotypes (Figure 7D). Production of CCL3 and CCL5 is significantly increased with LPS administration in both wildtype and knockout (Figure 7E, 7H), and LPS administration causes no change in the production of IL-18 (Figure 7F). Preliminary results also revealed significant up-regulation of RIP3 after systemic LPS administration in the wildtype mice (Figure 7I). These data demonstrate that systemic LPS administration causes significant increases of proinflammatory cytokine production in the developing brain and that ablation of RIP3 decreases brain production of TNF-α, IL-1β, CCL3 and CCL5. In summary, these data suggest that peripheral LPS sub cutaneous administration sufficiently induces central production of cytokines involved in inflammation and removal of RIP3 is sufficient to lower levels of cytokine production after LPS administration.

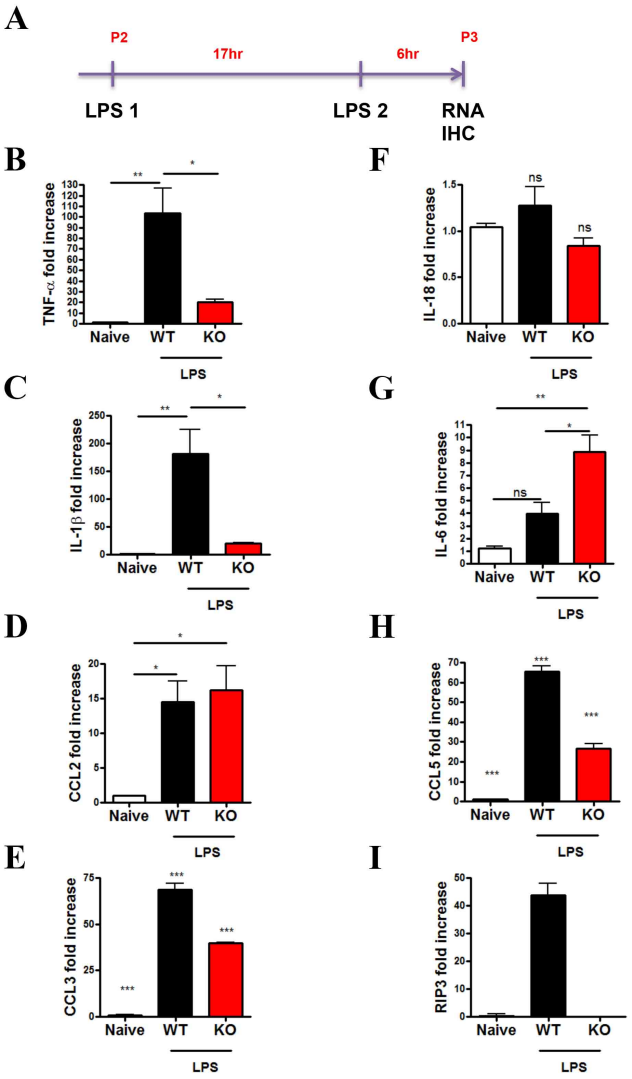

Figure 7 *Changes in proinflammatory cytokine transcript 24 hours after LPS administration.* (A) Timeline for two injections of LPS followed by tissue collection. (B) Significant increase in TNF-α transcript in wildtype animals 24 hours after LPS administration with a significant reduction in the RIP3$^{-/-}$ animals. (C) IL-1β transcript is significantly increased after LPS but is significantly reduced in RIP3 knockout. The chemokines CCL2 (D), CCL3 (E), and CCL5 (H) are similarly significantly increased after LPS administration in wildtype but not knockout mice. (F) IL-18 transcript remains unaltered after LPS administration. When injected with LPS, wildtype but not knockout animals increase RIP3 transcript. Finally, with IL-6 the opposite trend of significant increase of transcript in knockout but not wildtype is seen (G). Results are combined means $\pm$ SE *P<0.05, **P<0.01, ***P<0.001, ns not significant. Each group represents three mice from 6 independent experiments.

Immunohistochemistry (IHC) analysis reveals activated glia after systemic LPS administration

In parallel to findings at the transcript level, we next examined the brain using IHC and markers for astrocytes (GFAP) and microglia (Iba-1). Relative counts of Iba-1^{+} cells in the hippocampus revealed a significant increase in microglial activation after peripheral LPS administration. There is no significant difference in relative microglia number between genotypes (Figure 8A). Immunofluorescent images of the hippocampus region of naïve, wildtype, or knockout mice reveal lower numbers of microglia in naïve animals, but similar numbers between LPS administered wildtype and knockout animals (Figure 8B). Images of GFAP staining reveals increased expression of GFAP after LPS administration compared to naïve animals (Figure 8C). These results suggest that after LPS administration, expression of proinflammatory cytokines dramatically increases, microglia and astrocytes become activated, and proinflammatory cytokines are produced within 24 hours after LPS administration.

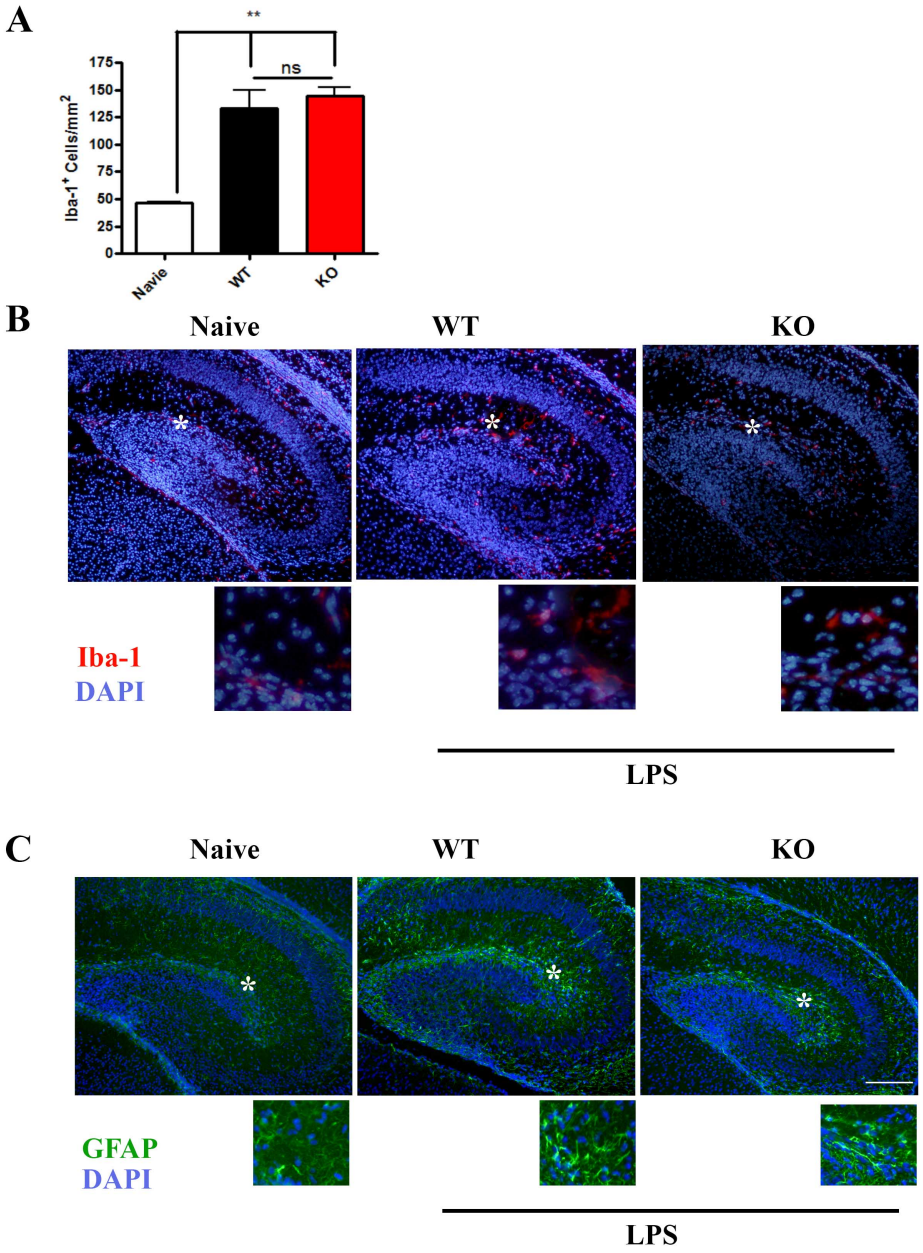

Figure 8 *Histology in the CNS of animals 24 hours after LPS administration*. Cells positive for Iba-1 are microglia while cells positive for GFAP are astrocytes. (A) Iba-1 positive cells show a significant increase in microglia in both groups administered LPS with no significant difference between wildtype and knockout animals. Representative images from each group showing microglial cells (B) or astrocytes (C). Results are combined means $\pm$ SE **P<0.01, ns not significant. Each group represents three mice from 6 independent experiments. Asterisk represents magnified region, shown below. Scale bar, 200 microns.

Brain inflammation after systemic LPS administration is largely subsided by 72 hours

We next examined the effect of hypoxia in combination of peripheral inflammation as it can lead to cerebral palsy, learning difficulties, and overall behavioral modifications. Here we asked if combination of LPS/hypoxia caused persistent gliosis and subsequent hypomyelination. We made modifications to our previous two-dose LPS administration experiment. Two days after hypoxia, the pups were taken from the dam and placed into a chamber that produced an 8% oxygen environment for 1 hour. The experimental timeline below details the entire process (Figure 9A). Next, we used half of the brain to extract RNA and examine cytokines and chemokines. We found almost no difference in cytokine transcript levels between wildtype and knockout animals after LPS administration. The following relative cytokine transcript levels of LPS administered animals show no difference between genotype: TNF-α, IL-18, IL-6, and CCL3 (Figure 9B, 9F, 9G, 9E). On the other hand, there appeared to be a noticeable difference when LPS was administered to the knockout animals compared to the wildtype for IL-1β, CCL2, and CCL5. Each of these appeared to be drastically reduced in knockout mice (Figure 9C, 9D, 9H). There were insufficient mouse numbers for all groups therefore significance was not established. These results suggest that inflammation and the resulting changes in cytokine and chemokine levels become resolved by 72 hours after the administration of LPS.

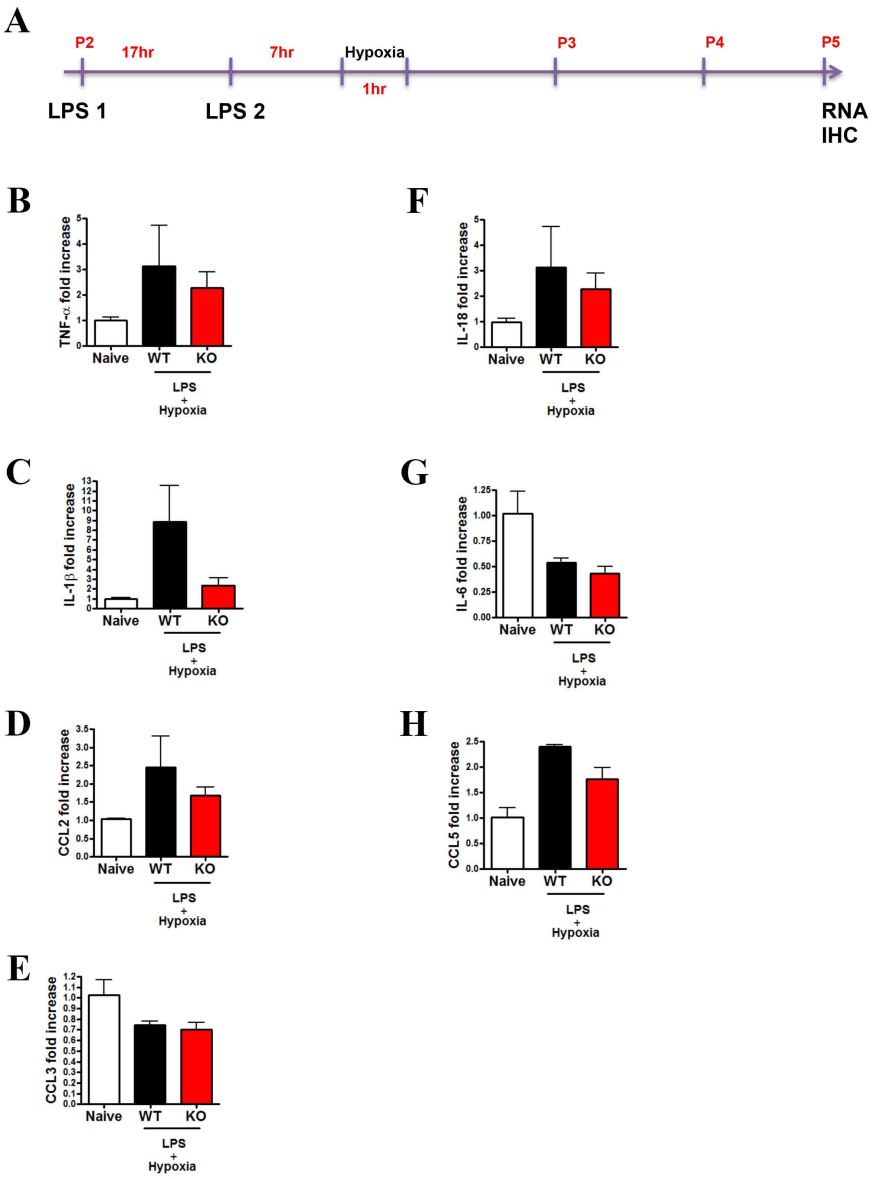

Figure 9 *Cytokine levels after LPS administration plus hypoxia*. (A) Timeline of experimental protocol. Preliminary pilot studies of animals injected with LPS followed by hypoxia and tissue collection 48 hours later show reduced increases in transcript. TNF-α (B), IL-1β (C), IL-18 (D) show higher increase in wildtype with lower increase in knockout while the chemokines CCL2 (F), CCL3 (G), CCL5 (H) show smaller to almost no increase compared to naïve and among LPS administered groups. The reversed trend seen in 24 hour injected animals is no longer different for IL-6 (E). No significance can be established, results representative of two independent experiments with two animals per group.

Comparable microgliosis between wildtype and RIP3 knockout mice 72 hours after LPS and hypoxia challenge

We again used IHC to determine the number of Iba-1 positive microglia cells. Nuclei that also have Iba-1 staining are considered to be microglia. An increase was seen in the relative number of microglial cells in the hippocampus in LPS-treated animals as compared to naïve mice. However, there was no difference between genotypes (Figure 10A). Representative immunofluorescence images for each group appear to have similar numbers of Iba-1 positive microglia in the hippocampus. Representative 10 x images are shown with an asterisk used to represent the zoomed in region shown magnified below (Figure 10B). These results suggest that subcutaneous LPS administration followed by 1 hour of hypoxia increased proliferation and/or activation of microglia in the hippocampus of the pup at postnatal day 6 to a similar extent in both genotypes.

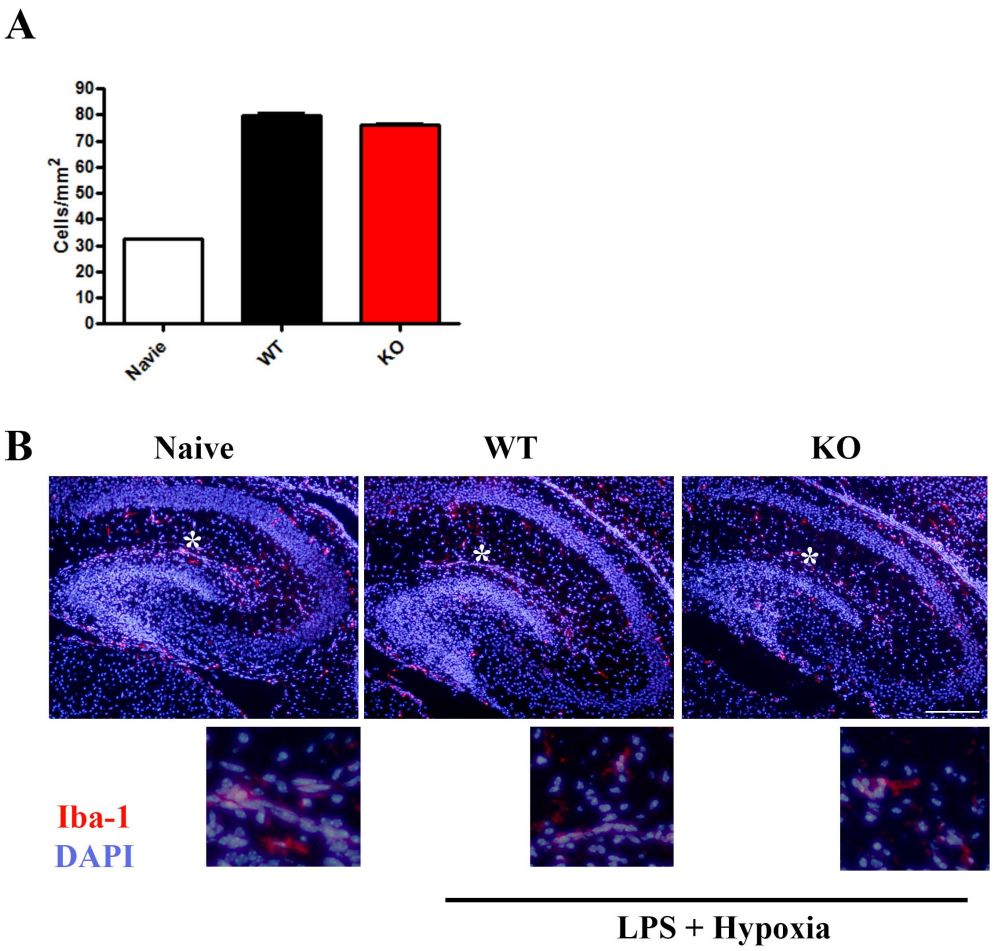

Figure 10 *Histology in the CNS of animals administered LPS 2 days after hypoxia*. (A) Iba-1 positive cells show an increase in microglia in both LPS administered groups with no difference between wildtype and knockout animals in a preliminary pilot run. Representative visual from each group showing microglia (B). No significance can be established, results representative of two independent experiments with two animals per group. Asterisk represents magnified region, shown below. Scale bar, 200 microns.

Long-term consequences of early postnatal systemic LPS challenge and transient hypoxia on the myelination program

CNS myelination occurs most robustly during postnatal week 2 and 3 in rodents, and we next asked if early inflammation and hypoxia affected CNS myelination by

examining three relevant genes. The experimental timeline is shown below (Figure 11A). After two doses of LPS followed by hypoxia, the pups were returned to the dam until weaning age at 21 days when they were sacrificed. There was no increase in proinflammatory cytokine levels at postnatal day 21 in treated mice when compared to non-treated naïve littermates (Figure 11B-H). Preliminary studies revealed that three of the genes responsible for myelination during normal CNS development appeared to be differentially expressed between treated wildtype and knockout animals. We observed an increase in 2',3'-Cyclic-nucleotide 3'-phosphodiesterase (CNP) transcript in the LPS administered knockout mice compared to naïve mice (Figure 12A). In addition, there was an increase in myelin basic protein (MBP) transcript levels in knockout animals administered LPS compared to naïve mice (Figure 12B). On the other hand, we noticed a reduction in myelin associated glycoprotein (MAG) transcript levels after LPS injection in the knockout mice (Figure 12C). Due to low number of mice in this experiment, further investigation is needed.

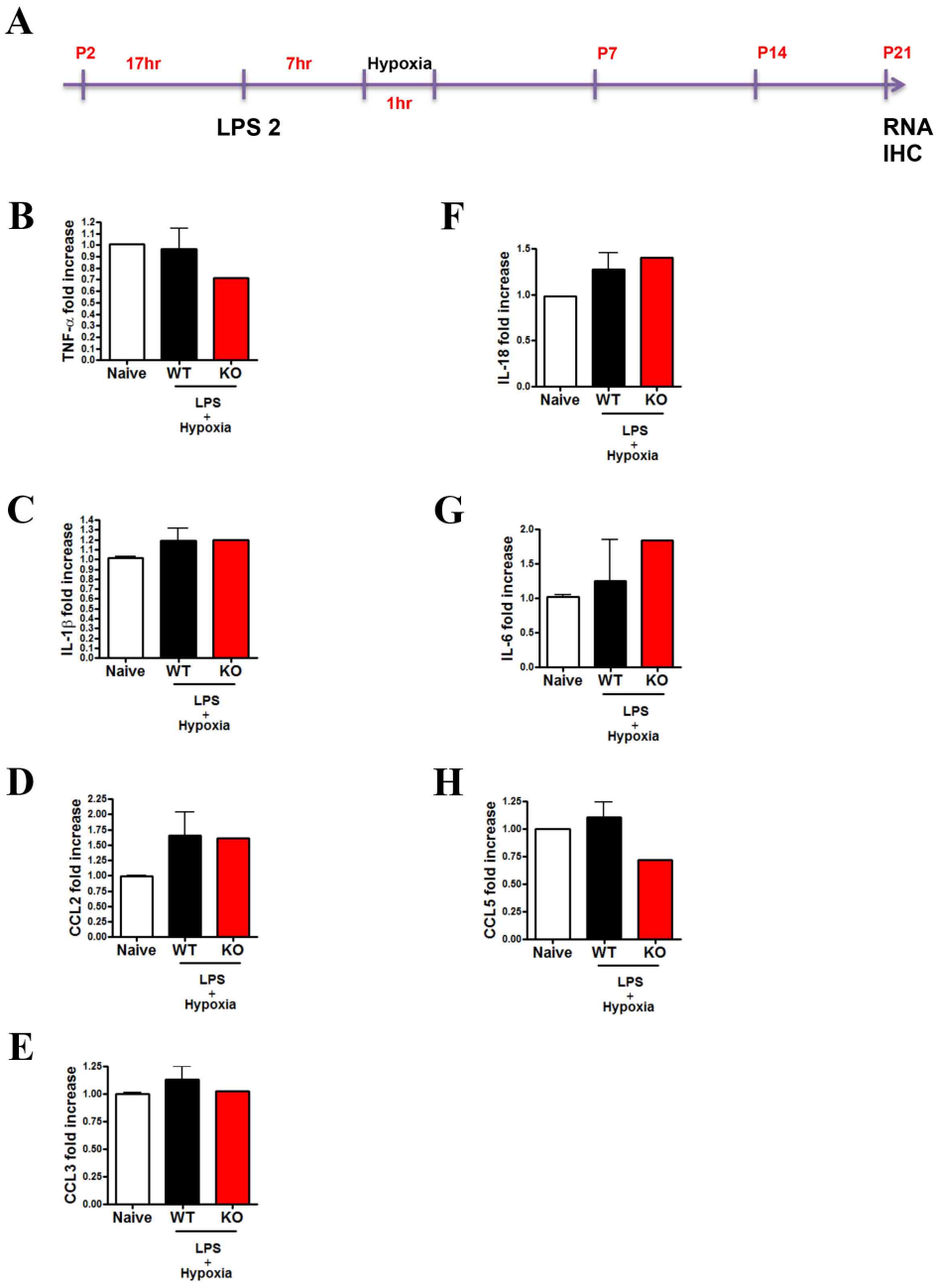

Figure 11 *Proinflammatory cytokine and chemokine transcripts in P21 mice after LPS administration at P2-P3*. (A) Experimental timeline. (B-E) cytokine levels are similar to naïve in all cytokines tested. No significance can be established, results representative of two independent experiments with two animals for naïve and wildtype and one animal for knockout.

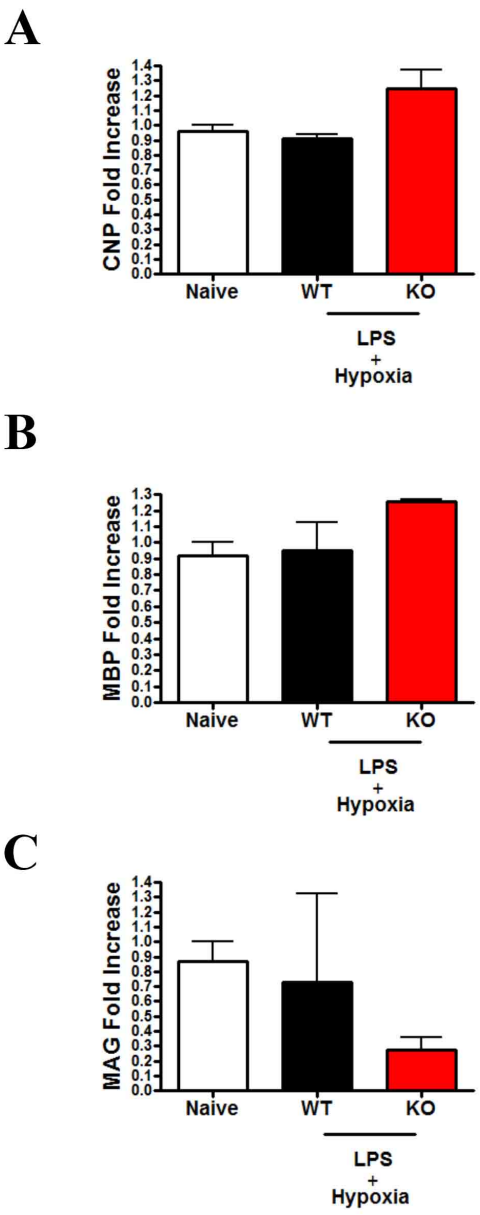

Figure 12 *Changes in transcript levels of myelination related genes at P21*. (A) Experimental timeline. Pilot study of animals injected with LPS spent 3 weeks developing. Transcript levels in genes responsible for myelination including CNP (B), MBP (C), and MAG (D) showed no major change among groups. No significance can be established, results representative of two independent experiments with two animals for naïve and wildtype and one animal for knockout.

Reduced number of $CC1^+$ oligodendrocytes in LPS injected wildtype mice compared to RIP3 knockout mice

CC1 labels post-mitotic maturing OLs and was used to analyze the effect of LPS plus hypoxia on CNS myelination. CC1 is a nuclear stain so that positive cells appear purple due to overlap of Hoechst 33342 in blue and CC1 in red. Littermate mice were challenged with LPS and hypoxia at P2-P4 as described earlier, and allowed to grow until weaning age, P21. Preliminary examination of the three groups (naïve, LPS/hypoxia wildtype (WT) and LPS/hypoxia knockout (KO)) revealed a reduction in the $CC1^+$ cell numbers for wildtype compared to naïve mice, but treated knockout mice had nearly the same number of $CC1^+$ cells per square millimeter as untreated naïve mice (Figure 13A). IHC and fluorescent images reveal the $CC1^+$ cell population in the hippocampus at P21 (Figure 13B). These results suggest that LPS administration early during development may result in fewer $CC1^+$ OLs when RIP3 is present.

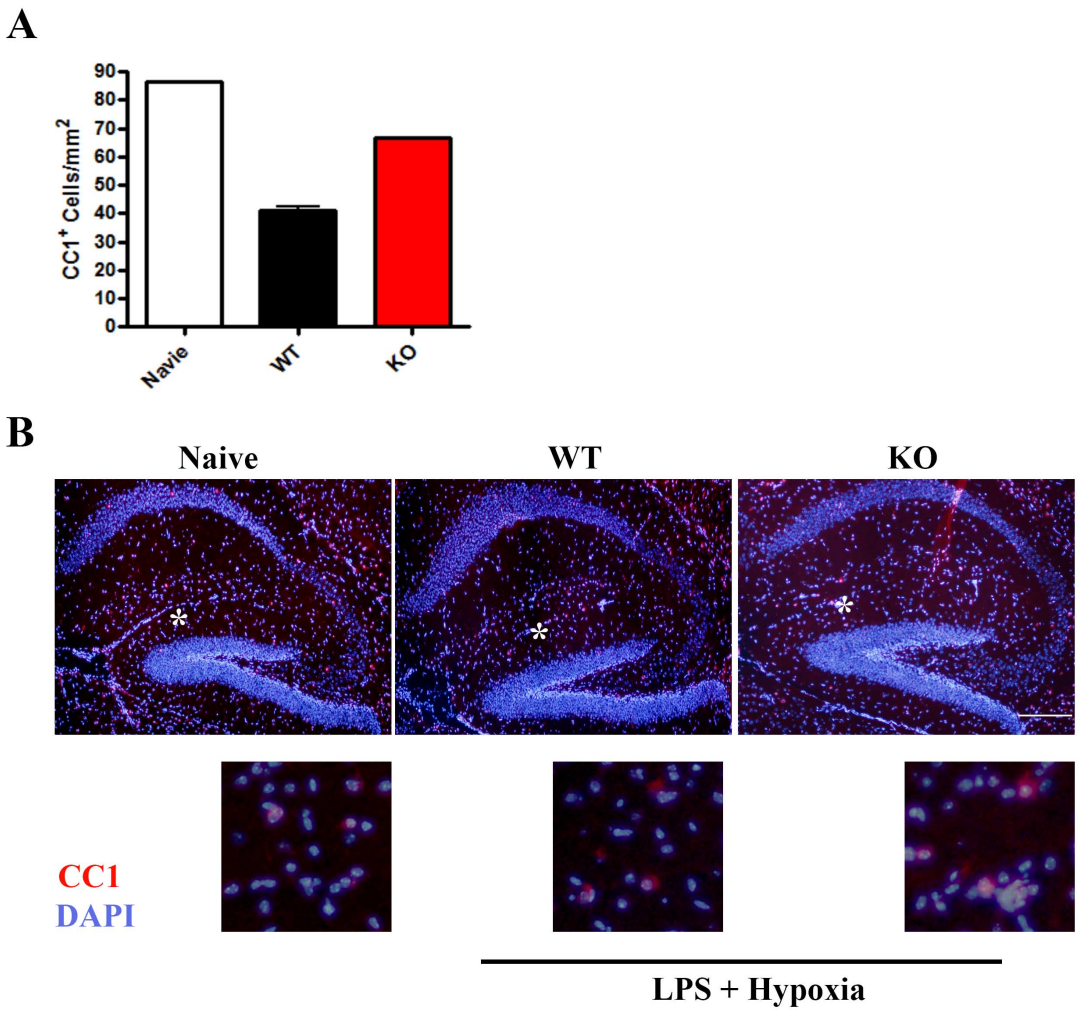

Figure 13 *Histology in the CNS of LPS injected animals at P21*. CC1 is an oligodendrocyte specific marker. (A) $CC1^+$ cells were counted from sagittal sections of the hippocampus region and little change was seen in both LPS administered groups (B) Representative visual from each group showing $CC1^+$ cells. No significance can be established, results representative of two independent experiments with two animals per group. Asterisk represents magnified region, shown below. Scale bar, 200 microns.

Changes in myelination in the hippocampus of P21 mice

In a pilot study, we used myelin proteolipid protein (PLP) immunohistochemistry to evaluate potential effects of early postnatal LPS challenge on myelination. There appears to be moderate differences between Naïve (Figure 14A), wildtype (Figure 14B),

and knockout mice (Figure 14C). However, due to limited number of mice used in these experiments, further study with additional numbers of mice for each group are needed.

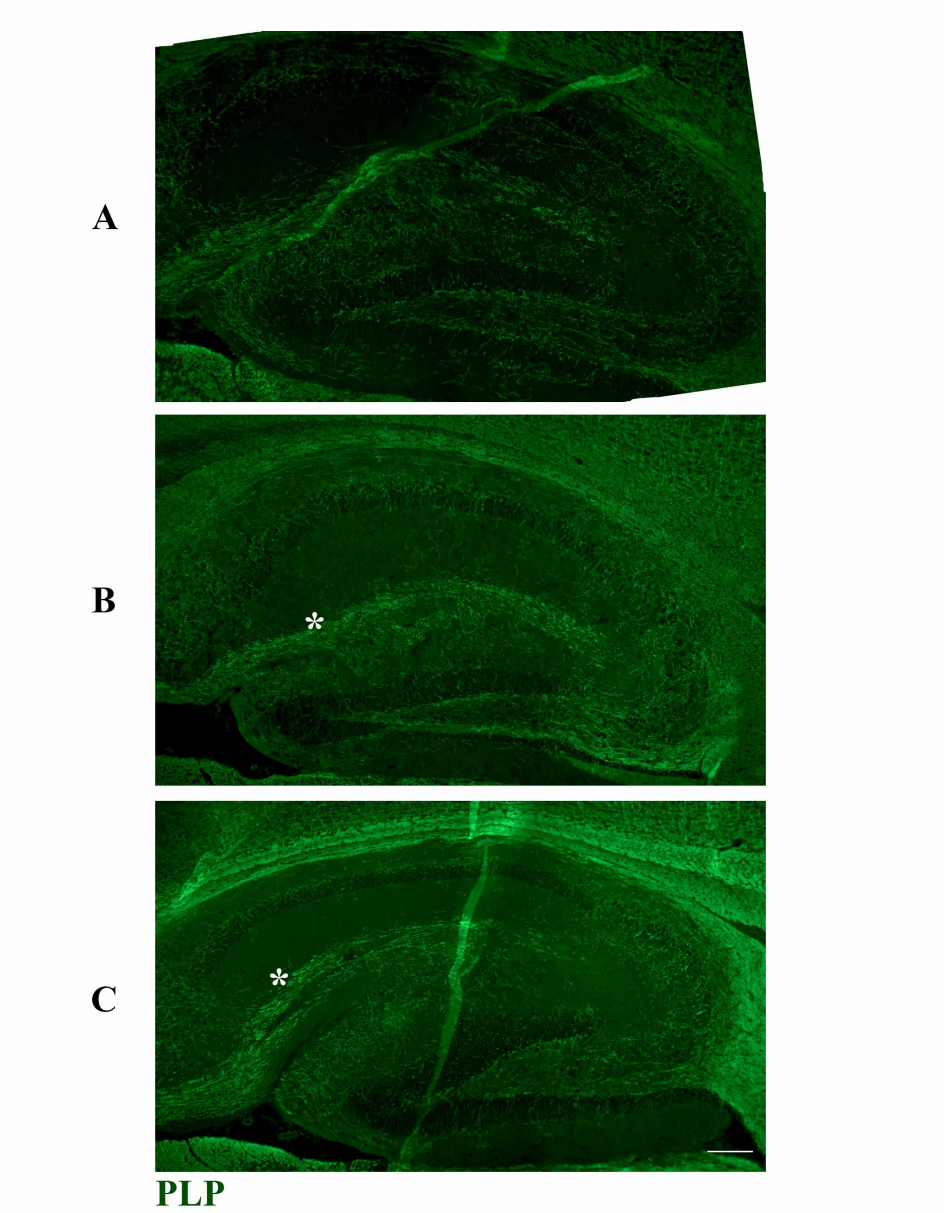

Figure 14 *Myelination program slightly altered by Hypoxia and LPS*. Three weeks after a combination of LPS and hypoxia, sagittal sections were sectioned and stained with PLP in Naïve (A), LPS/hypoxia treated wildtype (B) and LPS/hypoxia treated knockout (C) animals. Results representative of two experiments with one mouse per group. Asterisk denotes differences in myelination. Scale bar, 500 microns.

Organization of neurons in the hippocampus after LPS administration

We stained sagittal frozen sections of the hippocampus with cresyl violet (CV) and Hematoxylin and Eosin (H+E), which reveal nuclear bodies and the nissil substance found within nuclei respectively. Sections stained with H+E at 24 hours after LPS administration revealed expected hippocampal size and no dramatic reduction of neurons (Figure 15A). Two days after hypoxia and LPS injection, CV staining appears to show that some neurons are missing in CA1 region (Figure 15B). During the late time point (P21), the H+E staining shows a larger more developed hippocampus that appears unaltered (Figure 15C). These findings suggest that our experimental model of subcutaneous LPS administration and 1 hour of hypoxia does not cause overt disturbance in the overall neuronal structure and morphology of the hippocampus. Instead activation of glia and subsequent inflammation may lead to the consequences we have observed in these studies.

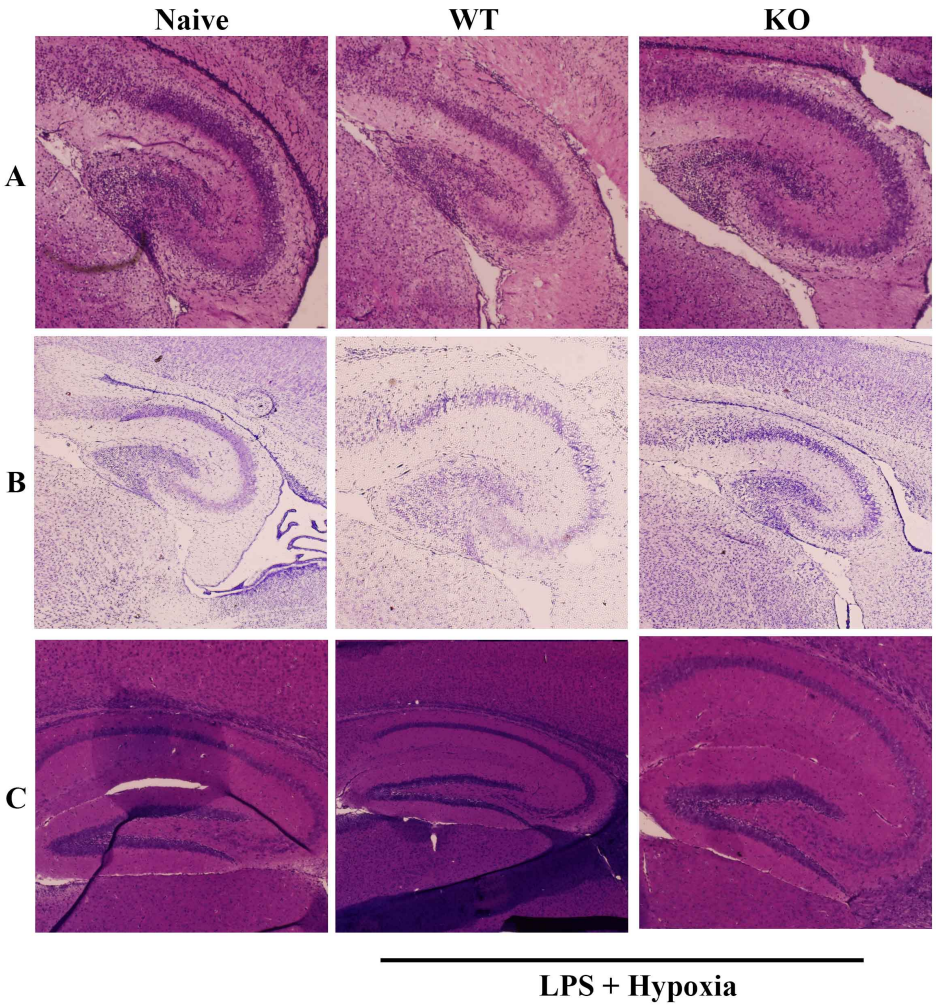

Figure 15 *Neuron staining in the hippocampus*. Frozen sagittal sections were stained using the H + E or CV methods. The hippocampus was still developing 24 hours after LPS injection at postnatal day 3 (A) with similar neuronal number and distribution. At postnatal day 5 (B), the hippocampus was further developed and larger with no major differences in neurons. Three weeks after injection at postnatal day 21 (C), the hippocampus was fully developed and larger with no change in neuron number. Representative images of three independent experiments with three mice per group.

CHAPTER IV

CONCLUSIONS

Central to maintaining a balance between cell death, inflammation, and programmed apoptotic cell death lie two key proteins. Historically, apoptosis has been the well-known form while the idea that programmed cell death could cause inflammation was not. Caspase 8 is a key protein for death receptor-mediated apoptosis and our recent work shows that RIP3 is involved with necroptosis in TLR-activated microglia in culture (Kim and Li, 2013), which could potentially lead to inflammation. Many studies have come to important conclusions involving both of these proteins. For example, structures termed inflammasomes are activated during infection and promote maturation of proinflammatory cytokine IL-1β. When caspase 8 is deleted, NLRP3 can assemble, a process that depends on RIP kinases (RIP1 & RIP3) (Kang et al., 2013). Other important findings include: inhibition of necroptosis by processing of CYLD-a substrate for proteolytic cleavage of caspase 8 (O'Donnell et al., 2011), inhibition of the synergistic complexes caspase-8-FLIP (L) which inhibits necrosis dependent on RIP3 (Oberst et al., 2011), and mediation of RIP3 and caspase 8's individual embryonic lethality (Kaiser et al., 2011). Finally, these two proteins have important roles in the immune system as noted during viral infection (Upton et al., 2010), and in T cell necroptotic mechanisms (Ch'en et al., 2011). Therefore caspase 8 and RIP3 are important factors to consider when events of inflammation events occur.

Very little is known about whether RIP3 regulates brain immunity. In this study, we present data demonstrating that within the first 24 hours after systemic administration of LPS, the CNS immune system is activated and RIP3 is up-regulated in the brain and contributes to the extent of inflammation. Future work examining removal of Caspase 8 and RIP3 in the CNS is vital for complete understanding of the findings obtained here. This family of receptor interacting proteins has been shown to involve themselves in mitochondrial integrity and oxidative stress (Rathinam et al., 2012, Wang et al., 2012). In the context of the nervous system, RIP3 has been shown to be involved in RIP-kinase mediated necrosis in photoreceptor cells (Trichonas et al., 2010) and is involved in rod and cone cell death which is triggered by kinase activity of RIP1/3 (Murakami et al., 2012). These exciting finding shed light on neuroinflammation and cell death mechanisms in the CNS. Besides the CNS, the function of RIP3 is implicated throughout the body. For example, macrophages circulating throughout the body responding to oxidized low density lipoprotein (LDL) have been shown to undergo necrosis mediated by RIP3 and this explosion of macrophages was shown to play a role in atherosclerosis development (Lin et al., 2013).

We demonstrated that neuron excitotoxicity in an ex vivo model of organotypic hippocampal slice culture can be reduced by removal of RIP3. Other studies examining RIP3 in other types of cells are newly emerging. For example, in the liver, many studies have implicated RIP3 in liver disease caused by acetaminophen toxicity (Luedde et al., 2014). RIP3 has also been implicated in lung injury (Zhao et al., 2014), and aortic abdominal aneurysm in necrosis of smooth muscle cells (Wang et al., 2015). The use of

genetic alteration by ablation, as used in this study, is one important approach to uncover important roles for RIP3. This is especially important due to a lack of inhibitors that are specific to RIP3. Necrostatin-1 is a compound that inhibits RIP1 activity and has been instrumental for our understanding of the role this family of proteins plays in the cell. It is important to note that Necrostatin-1 has been found to be involved in inhibiting activity of indoleamine-2,3-dioxygenase (IDO), an enzyme that catalyzes formation of tryptophan to kynurenine. As a result, two separate names were given to the same chemical compound (Vandenabeele et al., 2013). Our previous work reveals a role for Necrostatin-1 in preventing oxidative stress in oligodendrocytes (Kim et al., 2010). This compound is heavily used in the field and as an example, recent work has used it to show that receptor interacting proteins are involved in intracerebral hemorrhage induced brain injury (Su et al., 2015).

Preliminary studies outlined here show potential to help uncover new findings. For example, we show that early systemic inflammatory events may impact CNS myelination while others have shown that necrosis dependent on receptor interacting proteins drives lethal systemic inflammatory response syndrome (Duprez et al., 2011). Besides this broad array of findings, RIP3 has been implicated in weight loss regain in obese subjects (Goyenechea et al., 2009). Our study used two important approaches, an ex vivo slice culture model and an in vivo LPS hypoxia model to uncover the role RIP3 plays in regulating innate immunity and inflammation. Our findings in the ex vivo model show that slices lacking RIP3 after LPS preconditioned OGD have reduced neuronal excitotoxicity. It is likely that RIP3-dependent IL-1β production underlies LPS-induced

potentiation of OGD excitotoxicity. Our findings with the in vivo models show that inflammation in the CNS occurs within the first 24 hours after peripheral challenge and gradually diminishes to normal levels over time, which may affect the normal development of the brain.

In summary, our study was the first to use a genetic approach to investigate the role of RIP3 in inflammation and injury in the developing CNS. The microglia are the CNS resident cells that predominantly express RIP3. We found that ablation of RIP3 in our ex vivo model reduced CA1 excitotoxicity in OGD in slice cultures pre-treated with LPS. We also used an in vivo model system to administer LPS to early postnatal mice. This model revealed a role for RIP3 in producing increased levels of IL-1β immediately after LPS administration. From 72 hours after the LPS administration up until 21 days after, cytokine levels decreased over time to normal while other potential consequences remain to be examined.

REFERENCES

Ahn KS, Sethi G, Krishnan K, Aggarwal BB (2007) Gamma-tocotrienol inhibits nuclear factor-kappaB signaling pathway through inhibition of receptor-interacting protein and TAK1 leading to suppression of antiapoptotic gene products and potentiation of apoptosis. The Journal of biological chemistry 282:809-820.

Barks JD, Liu YQ, Shangguan Y, Li J, Pfau J, Silverstein FS (2008) Impact of indolent inflammation on neonatal hypoxic-ischemic brain injury in mice. International journal of developmental neuroscience : the official journal of the International Society for Developmental Neuroscience 26:57-65.

Ch'en IL, Tsau JS, Molkentin JD, Komatsu M, Hedrick SM (2011) Mechanisms of necroptosis in T cells. The Journal of experimental medicine 208:633-641.

Chavez-Valdez R, Martin LJ, Flock DL, Northington FJ (2012) Necrostatin-1 attenuates mitochondrial dysfunction in neurons and astrocytes following neonatal hypoxia-ischemia. Neuroscience 219:192-203.

Cho YS, Challa S, Moquin D, Genga R, Ray TD, Guildford M, Chan FK (2009) Phosphorylation-driven assembly of the RIP1-RIP3 complex regulates programmed necrosis and virus-induced inflammation. Cell 137:1112-1123.

Degterev A, Hitomi J, Germscheid M, Ch'en IL, Korkina O, Teng X, Abbott D, Cuny GD, Yuan C, Wagner G, Hedrick SM, Gerber SA, Lugovskoy A, Yuan J (2008) Identification of RIP1 kinase as a specific cellular target of necrostatins. Nature chemical biology 4:313-321.

Degterev A, Huang Z, Boyce M, Li Y, Jagtap P, Mizushima N, Cuny GD, Mitchison TJ, Moskowitz MA, Yuan J (2005) Chemical inhibitor of nonapoptotic cell death with therapeutic potential for ischemic brain injury. Nature chemical biology 1:112-119.

Duprez L, Takahashi N, Van Hauwermeiren F, Vandendriessche B, Goossens V, Vanden Berghe T, Declercq W, Libert C, Cauwels A, Vandenabeele P (2011) RIP kinase-dependent necrosis drives lethal systemic inflammatory response syndrome. Immunity 35:908-918

.

Favrais G, van de Looij Y, Fleiss B, Ramanantsoa N, Bonnin P, Stoltenburg-Didinger G, Lacaud A, Saliba E, Dammann O, Gallego J, Sizonenko S, Hagberg H, Lelievre

V, Gressens P (2011) Systemic inflammation disrupts the developmental program of white matter. Annals of neurology 70:550-565.

Finkel T, Holbrook NJ (2000) Oxidants, oxidative stress and the biology of ageing. Nature 408:239-247.

Goyenechea E, Crujeiras AB, Abete I, Martinez JA (2009) Expression of two inflammation-related genes (RIPK3 and RNF216) in mononuclear cells is associated with weight-loss regain in obese subjects. Journal of nutrigenetics and nutrigenomics 2:78-84.

He S, Wang L, Miao L, Wang T, Du F, Zhao L, Wang X (2009) Receptor interacting protein kinase-3 determines cellular necrotic response to TNF-alpha. Cell 137:1100-1111.

Kaindl AM, Degos V, Peineau S, Gouadon E, Chhor V, Loron G, Le Charpentier T, Josserand J, Ali C, Vivien D, Collingridge GL, Lombet A, Issa L, Rene F, Loeffler JP, Kavelaars A, Verney C, Mantz J, Gressens P (2012) Activation of microglial N-methyl-D-aspartate receptors triggers inflammation and neuronal cell death in the developing and mature brain. Annals of neurology 72:536-549.

Kaiser WJ, Upton JW, Long AB, Livingston-Rosanoff D, Daley-Bauer LP, Hakem R, Caspary T, Mocarski ES (2011) RIP3 mediates the embryonic lethality of caspase-8-deficient mice. Nature 471:368-372.

Kang TB, Yang SH, Toth B, Kovalenko A, Wallach D (2013) Caspase-8 blocks kinase RIPK3-mediated activation of the NLRP3 inflammasome. Immunity 38:27-40.

Kasof GM, Prosser JC, Liu D, Lorenzi MV, Gomes BC (2000) The RIP-like kinase, RIP3, induces apoptosis and NF-kappaB nuclear translocation and localizes to mitochondria. FEBS letters 473:285-291.

Kim S, Dayani L, Rosenberg PA, Li J (2010) RIP1 kinase mediates arachidonic acid-induced oxidative death of oligodendrocyte precursors. International journal of physiology, pathophysiology and pharmacology 2:137-147.

Kim SJ, Li J (2013) Caspase blockade induces RIP3-mediated programmed necrosis in Toll-like receptor-activated microglia. Cell death & disease 4:e716.

Lin J, Li H, Yang M, Ren J, Huang Z, Han F, Huang J, Ma J, Zhang D, Zhang Z, Wu J, Huang D, Qiao M, Jin G, Wu Q, Huang Y, Du J, Han J (2013) A role of RIP3-mediated macrophage necrosis in atherosclerosis development. Cell reports 3:200-210.

Linkermann A, Brasen JH, Himmerkus N, Liu S, Huber TB, Kunzendorf U, Krautwald S (2012) Rip1 (receptor-interacting protein kinase 1) mediates necroptosis and contributes to renal ischemia/reperfusion injury. Kidney international 81:751-761.

Livak KJ, Schmittgen TD (2001) Analysis of relative gene expression data using real-time quantitative PCR and the 2(-Delta Delta C(T)) Method. Methods 25:402-408.

Loron G, Olivier P, See H, Le Sache N, Angulo L, Biran V, Brunelle N, Besson-Lescure B, Kitzis MD, Pansiot J, Bingen E, Gressens P, Bonacorsi S, Baud O (2011) Ciprofloxacin prevents myelination delay in neonatal rats subjected to E. coli sepsis. Annals of neurology 69:341-351.

Luedde T, Kaplowitz N, Schwabe RF (2014) Cell death and cell death responses in liver disease: mechanisms and clinical relevance. Gastroenterology 147:765-783 e764.

Mallard C, Wang X (2012) Infection-induced vulnerability of perinatal brain injury. Neurology research international 2012:102153.

Murakami Y, Matsumoto H, Roh M, Suzuki J, Hisatomi T, Ikeda Y, Miller JW, Vavvas DG (2012) Receptor interacting protein kinase mediates necrotic cone but not rod cell death in a mouse model of inherited degeneration. Proceedings of the National Academy of Sciences of the United States of America 109:14598-14603.

Newton K, Sun X, Dixit VM (2004) Kinase RIP3 is dispensable for normal NF-kappa Bs, signaling by the B-cell and T-cell receptors, tumor necrosis factor receptor 1, and Toll-like receptors 2 and 4. Molecular and cellular biology 24:1464-1469.

Nobuta H, Ghiani CA, Paez PM, Spreuer V, Dong H, Korsak RA, Manukyan A, Li J, Vinters HV, Huang EJ, Rowitch DH, Sofroniew MV, Campagnoni AT, de Vellis J, Waschek JA (2012) STAT3-mediated astrogliosis protects myelin development in neonatal brain injury. Annals of neurology 72:750-765.

Northington FJ, Chavez-Valdez R, Graham EM, Razdan S, Gauda EB, Martin LJ (2011) Necrostatin decreases oxidative damage, inflammation, and injury after neonatal HI. Journal of cerebral blood flow and metabolism : official journal of the International Society of Cerebral Blood Flow and Metabolism 31:178-189.

O'Donnell MA, Perez-Jimenez E, Oberst A, Ng A, Massoumi R, Xavier R, Green DR, Ting AT (2011) Caspase 8 inhibits programmed necrosis by processing CYLD. Nature cell biology 13:1437-1442.

Oberst A, Dillon CP, Weinlich R, McCormick LL, Fitzgerald P, Pop C, Hakem R, Salvesen GS, Green DR (2011) Catalytic activity of the caspase-8-FLIP(L) complex inhibits RIPK3-dependent necrosis. Nature 471:363-367.

Oerlemans MI, Liu J, Arslan F, den Ouden K, van Middelaar BJ, Doevendans PA, Sluijter JP (2012) Inhibition of RIP1-dependent necrosis prevents adverse cardiac remodeling after myocardial ischemia-reperfusion in vivo. Basic research in cardiology 107:270.

Ofengeim D, Yuan J (2013) Regulation of RIP1 kinase signalling at the crossroads of inflammation and cell death. Nature reviews Molecular cell biology 14:727-736.

Pazdernik NJ, Donner DB, Goebl MG, Harrington MA (1999) Mouse receptor interacting protein 3 does not contain a caspase-recruiting or a death domain but induces apoptosis and activates NF-kappaB. Molecular and cellular biology 19:6500-6508.

Rathinam VA, Vanaja SK, Waggoner L, Sokolovska A, Becker C, Stuart LM, Leong JM, Fitzgerald KA (2012) TRIF licenses caspase-11-dependent NLRP3 inflammasome activation by gram-negative bacteria. Cell 150:606-619.

Rousset CI, Chalon S, Cantagrel S, Bodard S, Andres C, Gressens P, Saliba E (2006) Maternal exposure to LPS induces hypomyelination in the internal capsule and programmed cell death in the deep gray matter in newborn rats. Pediatric research 59:428-433.

Rousset CI, Kassem J, Aubert A, Planchenault D, Gressens P, Chalon S, Belzung C, Saliba E (2013) Maternal exposure to lipopolysaccharide leads to transient motor dysfunction in neonatal rats. Developmental neuroscience 35:172-181.

Sheldon RA, Jiang X, Francisco C, Christen S, Vexler ZS, Tauber MG, Ferriero DM (2004) Manipulation of antioxidant pathways in neonatal murine brain. Pediatric research 56:656-662.

Shrivastava K, Chertoff M, Llovera G, Recasens M, Acarin L (2012) Short and long-term analysis and comparison of neurodegeneration and inflammatory cell response in the ipsilateral and contralateral hemisphere of the neonatal mouse brain after hypoxia/ischemia. Neurology research international 2012:781512.

Su X, Wang H, Kang D, Zhu J, Sun Q, Li T, Ding K (2015) Necrostatin-1 Ameliorates Intracerebral Hemorrhage-Induced Brain Injury in Mice Through Inhibiting RIP1/RIP3 Pathway. Neurochemical research.

Sun X, Lee J, Navas T, Baldwin DT, Stewart TA, Dixit VM (1999) RIP3, a novel apoptosis-inducing kinase. The Journal of biological chemistry 274:16871-16875.

Sun X, Yin J, Starovasnik MA, Fairbrother WJ, Dixit VM (2002) Identification of a novel homotypic interaction motif required for the phosphorylation of receptor-interacting protein (RIP) by RIP3. The Journal of biological chemistry 277:9505-9511.

Sundstrom L, Morrison B, 3rd, Bradley M, Pringle A (2005) Organotypic cultures as tools for functional screening in the CNS. Drug discovery today 10:993-1000.

Trichonas G, Murakami Y, Thanos A, Morizane Y, Kayama M, Debouck CM, Hisatomi T, Miller JW, Vavvas DG (2010) Receptor interacting protein kinases mediate retinal detachment-induced photoreceptor necrosis and compensate for inhibition of apoptosis. Proceedings of the National Academy of Sciences of the United States of America 107:21695-21700.

Upton JW, Kaiser WJ, Mocarski ES (2010) Virus inhibition of RIP3-dependent necrosis. Cell host & microbe 7:302-313.

Vandenabeele P, Declercq W, Van Herreweghe F, Vanden Berghe T (2010a) The role of the kinases RIP1 and RIP3 in TNF-induced necrosis. Science signaling 3:re4.

Vandenabeele P, Galluzzi L, Vanden Berghe T, Kroemer G (2010b) Molecular mechanisms of necroptosis: an ordered cellular explosion. Nature reviews Molecular cell biology 11:700-714.

Vandenabeele P, Grootjans S, Callewaert N, Takahashi N (2013) Necrostatin-1 blocks both RIPK1 and IDO: consequences for the study of cell death in experimental disease models. Cell death and differentiation 20:185-187.

Wang Q, Liu Z, Ren J, Morgan S, Assa C, Liu B (2015) Receptor-Interacting Protein Kinase 3 Contributes to Abdominal Aortic Aneurysms via Smooth Muscle Cell Necrosis and Inflammation. Circulation research 116:600-611.

Wang Z, Jiang H, Chen S, Du F, Wang X (2012) The mitochondrial phosphatase PGAM5 functions at the convergence point of multiple necrotic death pathways. Cell 148:228-243.

Yu PW, Huang BC, Shen M, Quast J, Chan E, Xu X, Nolan GP, Payan DG, Luo Y (1999) Identification of RIP3, a RIP-like kinase that activates apoptosis and NFkappaB. Current biology : CB 9:539-542.

Zhang DW, Shao J, Lin J, Zhang N, Lu BJ, Lin SC, Dong MQ, Han J (2009) RIP3, an energy metabolism regulator that switches TNF-induced cell death from apoptosis to necrosis. Science 325:332-336.

Zhao H, Ning J, Lemaire A, Koumpa FS, Sun JJ, Fung A, Gu J, Yi B, Lu K, Ma D (2014) Necroptosis and parthanatos are involved in remote lung injury after receiving ischemic renal allografts in rats. Kidney international.